Statistical Bit Error Trace Modeling of Acoustic Communication Links Using Decision Feedback Equalization

Mandar Chitre, *Senior Member, IEEE*, Konstantinos Pelekanakis, *Member, IEEE*, and Matthew Legg, *Member, IEEE*

***Abstract*—Underwater network simulation and performance analysis require accurate packet error models. The packet error probability depends on the packet length and the temporal distribution of bit errors. We analyze error traces from decision-feedback-equalized single-carrier acoustic communication links from several shallow-water experiments and show that clustering of bit errors occurs at several timescales. We propose a two-part statistical error model consisting of a generalized Pareto fractal renewal parent process that drives Bernoulli daughter processes with generalized extreme value distributed lifetimes. We present an algorithm to simulate communication errors using this error process model and show that the simulated packet loss probability accurately matches experimental observations.**

***Index Terms*—Bit errors, generalized Pareto renewal process, packet errors, underwater communications.**

I. Introduction

UNDERWATER communication performance in terms of data rate and robustness has improved significantly over the past few decades. Underwater acoustic modem technology has, therefore, matured to a level where underwater networks can be deployed and tested. However, the cost, logistics, and effort involved in deploying experimental underwater networks remains high, and is beyond the reach of many researchers. Even researchers who have access to resources for experimental research in underwater networks prefer to test their networks in simulation before experimental testing. Hence, the need for accurate underwater network simulators is key to the future of underwater networking research.

Some underwater networking researchers have customized network simulators (e.g., Omnet++, Opnet, Qualnet, ns-2) while others have chosen to develop their own discrete event simulators. More recently, the idea of simulating and experimentally testing underwater protocols with identical implementations (source code) has become popular [1]–[4]. In all of the cases, an underwater physical layer performance model is required by the simulator to model the packet loss performance for each link in the network. Although sophisticated physics-based time-varying channel models can be used to determine the errors in each transmitted packet, this approach is computationally infeasible for large-scale simulation. Rather than compute the errors for each packet, some simulators [e.g., world ocean simulation system (WOSS)] use acoustic propagation modeling to estimate the packet loss probability [5]. The packet loss probability is then used to simulate packet errors. This provides a feasible solution for static networks but the computational load in case of mobile networks is prohibitively large as the acoustic modeling has to be performed every time a node moves. In addition, the computationally feasible physical models may not model all the factors affecting communication performance and, therefore, may not be able to model the variability in the channel accurately. To reduce complexity further, some researchers use simple range-dependent packet loss probability to model the performance of each link [1]. The computation of the packet loss probability assumes independent bit errors and a constant probability of bit error for a given range. Although useful as a first-order approximation with very low computational complexity, this approach fails to capture the time variability in the channel and the consequent clustering of errors that occurs in underwater channels. Statistical finite state Markov models have been used to model time variability in packet loss rates [6], [7]. Hidden Markov models have been shown to model the packet loss of the JANUS modulation scheme during a specific experiment [7], yet it is not known if these models are generally applicable. Moreover, since the packet error rate (PER) depends on packet size, distinct models are required for different packet sizes.

To partially alleviate the problems described above, we apply statistical modeling to bit errors rather than packet loss. Specifically, we statistically characterize bit error traces from a channel-estimate-based decision feedback equalizer (CEB–DFE) by analyzing signals from the SPACE'08 experiment. Using the data collected, we propose a statistical model for the occurrence of errors in a data stream. We further validate this model by using data from the RACE'08 and ROMANIS'10 experiments. This model can then be used to compute realistic time-varying packet loss probability for use in analytical network performance modeling and network simulation.

The rest of this paper is organized as follows. In Section II, we describe the SPACE'08 experiment and data processing that led

Manuscript received December 02, 2012; revised February 28, 2013; accepted April 04, 2013. Date of publication July 18, 2013; date of current version October 09, 2013.

Guest Editor: M. Porter.

M. Chitre is with the Electrical & Computer Engineering Department and the Acoustic Research Laboratory (ARL), National University of Singapore, Singapore 119227, Singapore (e-mail: mandar@arl.nus.edu.sg).

K. Pelekanakis and M. Legg are with the Acoustic Research Laboratory (ARL), National University of Singapore, Singapore 119227, Singapore (e-mail: costas@arl.nus.edu.sg; legg@ieee.org).

Color versions of one or more of the figures in this paper are available online at http://ieeexplore.ieee.org.

Digital Object Identifier 10.1109/JOE.2013.2257571

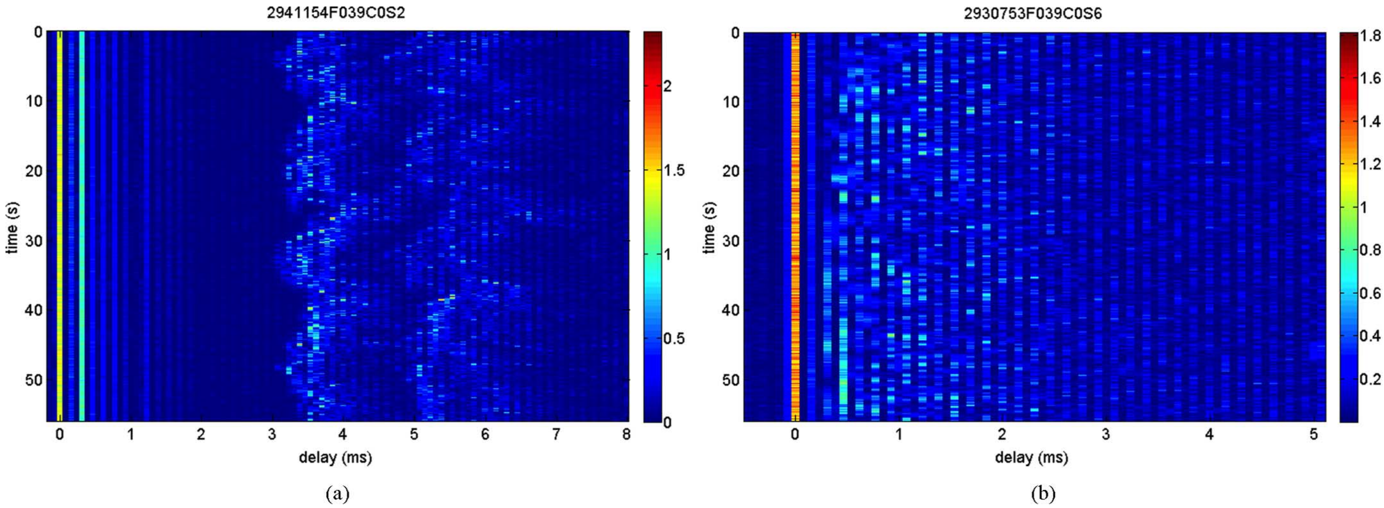

Fig. 1. Representative impulse responses from the (a) 80-m and (b) 1-km links during the SPACE'08 experiment. The horizontal axis represents multipath delay and the vertical axis represents absolute time. The colorbar is in a linear scale. The snapshots are generated at the bit rate.

to the bit error traces. Using Fano factor analysis, a well-established technique for measuring clustering [8], we show that the error traces exhibit clustering at several scales and demonstrate the effect of this on packet loss probability. We show that the long timescale clustering can be modeled using a fractal renewal process, while shorter timescale clustering can be approximated by a limited lifetime Bernoulli process. A renewal process is characterized by independent intervals between events. We use the serial correlation coefficient to demonstrate independence of the measured intervals between errors. We use statistical tools such as confidence intervals of the cumulative hazard function, Berman's test, and Kolmogorov–Smirnov test to show that the long timescale process model fits the experimental data well. The distribution of lifetime of the short timescale process is characterized. In Section III, we integrate our findings into a statistical model for the error process. We show that this model predicts experimentally observed packet loss probability accurately. We also show that second-order statistics can also be predicted using the model. In Section IV, we validate the proposed model using data from several experiments. Finally, in Section V, we discuss the implications of this model as well as some of its shortcomings. We also suggest directions for further research in this area.

II. SPACE'08 Data Analysis

A. Data Collection

The first set of experimental data that we use in this paper was recorded during the SPACE'08 experiment off the coast of Martha's Vineyard, MA, USA, in 2008. The transmitter and the receiver were static and were located 4 and 3.25 m, respectively, above the seafloor. The water depth was about 15 m. The transmitted signal was a 6510.4-b/s binary phase-shift keying (BPSK) pseudonoise (PN) sequence that was modulated onto a 12.5-kHz carrier. The source level was 185 dB re 1 μPa @ 1 m. Data from two horizontal ranges (80 and 1000 m) were used in the analysis presented in this paper.

The receiver employed CEB–DFE, namely, the intersymbol interference (ISI) was canceled by combining previous channel and symbol decisions before adaptive feedforward (FF) equalization. Channel estimation was performed by employing a novel sparse adaptive algorithm [9]. The FF equalizer was adapted to channel variations via the recursive least square (RLS) algorithm. Representative impulse responses for the channels are shown in Fig. 1.

The demodulated data were compared with the transmitted PN sequence to form error traces. Each error trace was generated from a 1-min data set with about 3.6×10^5 b. The error trace was only collected once the equalizer switched to a decision-directed mode after an initial training period of 500 b. Three error traces (denoted by F38S2DD, F39S2DD, and F40S2DD) were obtained for the 80-m channel, and another three error traces (F38S6DD, F39S6DD, and F40S6DD) were obtained for the 1-km channel. In the decision-directed mode, we expected some error feedback leading to error propagation in the traces. To guide our understanding of the underlying error generation process with minimal error feedback, we also generated error trace data for the equalizer running in training mode for the entire data set. These training mode error traces corresponding to F38S2DD, F39S2DD, and F40S2DD are denoted by F38S2TR, F39S2TR, and F40S2TR, respectively.

B. Bernoulli Error Process Model

As a first-order approximation, the bit error trace can be modeled as a Bernoulli process with a constant and independent probability b of bit error. In this model, the number of bit errors in a window of size n bits follows a Binomial distribution with mean nb and variance $nb(1-b)$. The ratio of the variance to the mean of the finite interval count distribution of a point process is known as the normalized variance or Fano factor [8]. The Fano factor is a measure of clustering, and, therefore, a useful statistic to identify data consistent with Poisson arrival, Bernoulli, and fractal renewal processes. For a Binomial distribution, the Fano factor is $1/(1-b)$ and, therefore, independent of the window size n. For small b, the Fano factor is expected to be close to 1. The Fano factors for the six decision-directed error traces are shown in Fig. 2. The Fano factors for all error traces are clearly

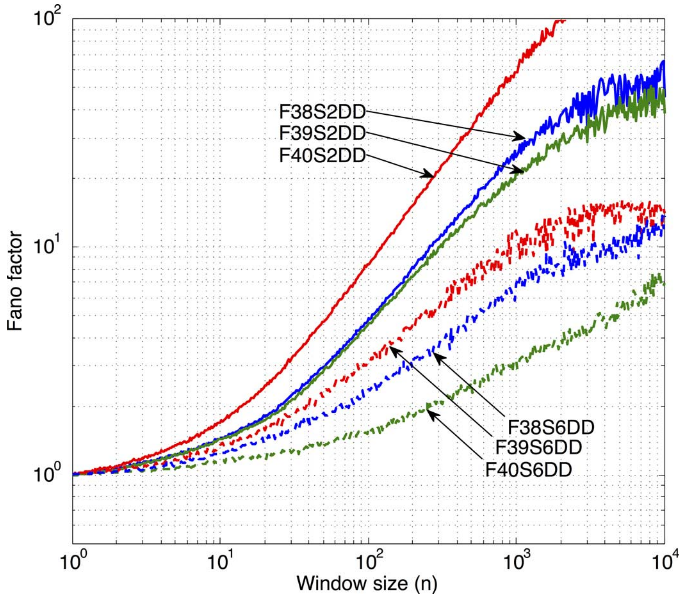

Fig. 2. Fano factor plot of error traces in decision-directed mode.

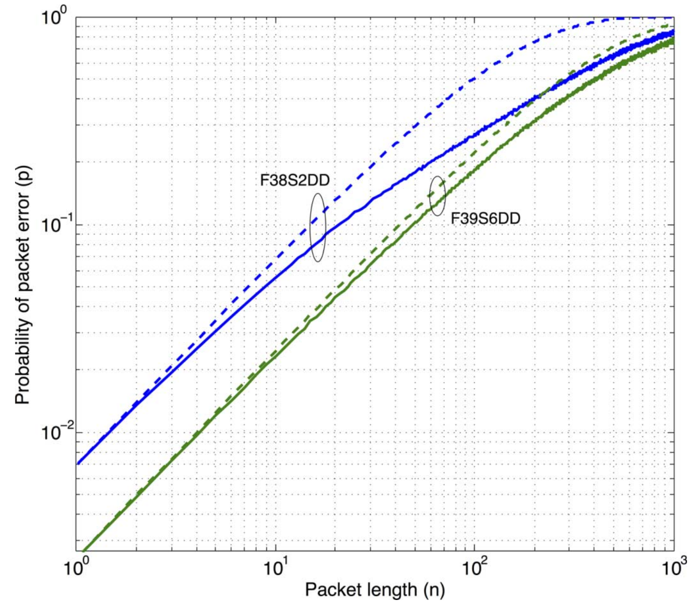

Fig. 3. Probability of packet error for two decision-directed error traces (one each from the 80-m and 1-km channels). The solid line shows the estimated packet error probability from the error trace, while the dashed line shows the corresponding packet error probability predicted by the Bernoulli error model with an estimated bit error probability.

dependent on n. For large n, the Fano factors are much larger than 1 suggesting clustered occurrence of errors.

The error count distribution in a window is directly related to the probability of packet error. A packet of length n is successfully received if there are no bit errors in the packet. For a Bernoulli error process, the probability p of packet error is, therefore, given by

$$p = 1 - (1 - b)^n. \quad (1)$$

By dividing an error trace into nonoverlapping packets of n bits each and counting what fraction of the packets are error free, we can obtain an estimate of the packet error probability p. In Fig. 3, we compare the estimated packet error probability with the prediction from the Bernoulli model for two representative error traces. The Bernoulli model for each of the error traces uses a bit error probability estimate $b = E/N$, where E is the total number of errors and N is the total number of bits in that trace. At short packet lengths, the model provides a good estimate of packet error probability, but as the packet length increases, the predicted probability deviates from the observed probability. This can be understood in terms of the Fano factor. At short window sizes, the Fano factor is close to unity. This is consistent with a Binomial distribution for the number of errors in the window, and thus a Bernoulli model for the error process at this packet length scale is a good approximation. As the window size increases, the Fano factor grows rapidly. This growth indicates a deviation from the Bernoulli model and results in a model mismatch with observations. The large Fano factor at these window sizes is indicative of a clustering of errors; the Bernoulli model, therefore, overestimates the packet error probability.

From the above analysis, we see that the Bernoulli process is a poor model for the errors in our data sets. The observed errors are clustered more tightly than the Bernoulli model predicts. One possibility is that variations of the acoustic channel over short timescales (our data set is only 1 min long) may give rise to time-varying error probability. Another possibility is that the decision feedback process in the decision-directed mode may temporarily increase the error probability once an error occurs. To differentiate between these two possibilities, next we study the training mode error traces.

C. *Training Mode Errors*

In the decision-directed mode, erroneous decision feedback in the receiver potentially leads to error clusters over short timescales. To understand how much of the observed deviation from the Bernoulli model is due to this effect, we study the Fano factor plots for the training error traces (see Fig. 4). The Fano factor curves significantly differ from those in Fig. 2. For small values of n, the Fano factor for the training error traces stays close to 1. Thus, a Bernoulli process with a small bit error probability seems to model our training error traces at very short timescales, suggesting that erroneous decision feedback is primarily responsible for the observed error clustering over these timescales. The increase in Fano factors at larger n indicates clustering at longer timescales due to variability in the acoustic channel.

D. *Fractal Renewal Process Model*

A renewal process is a point process where the interval between adjacent events (errors) is independent and identically distributed (i.i.d.). A fractal renewal process is a renewal process where the interval distribution exhibits self-similarity at different timescales. The concept of self-similarity for a point process can be understood in terms of the scaling of the statistics of the process [10], specifically, the statistics used

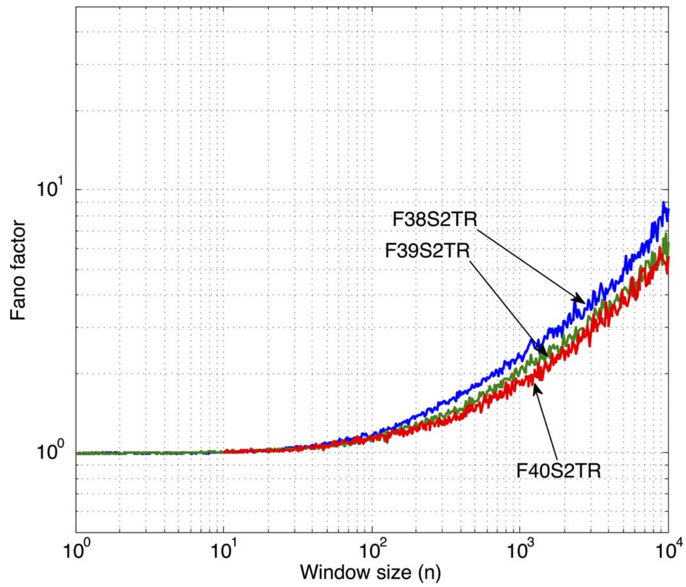

Fig. 4. Fano factor plot of error traces in training mode.

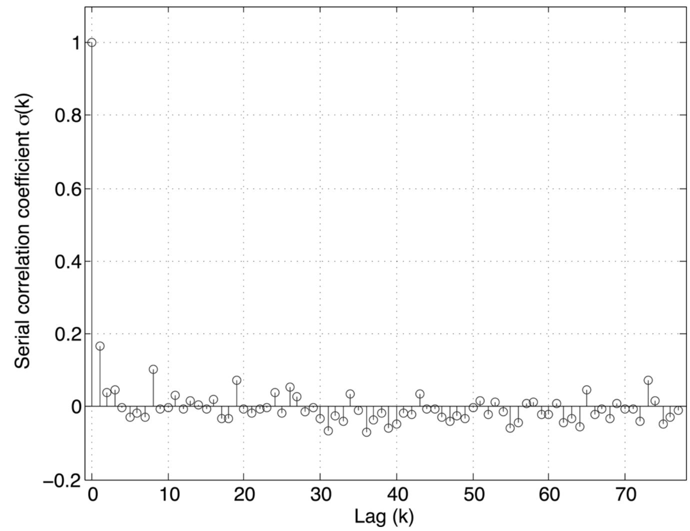

Fig. 5. Interval serial correlation coefficient $\sigma(k)$ for a filtered F38S2DD error trace with $T = 50$ b. The serial correlation coefficient plots for other filtered error traces look very similar.

to describe the process scale with the window size employed. The shape of the Fano factor curves in Fig. 4 is characteristic of Fano factor curves for fractal renewal processes [10], [11]. Inspired by this similarity, we next explore whether a fractal renewal process is able to model the longer timescale error clustering due to channel variability.

As this section focuses on the longer timescale clustering due to channel variability, we start by filtering the decision-directed error traces to remove short-term clustering due to erroneous decision feedback. Let $\{t_i \ \forall \ i \in \mathbb{N}_0\}$ be the set of error locations in the error trace, ordered such that $t_{i-1} < t_i$. Let the interval $\tau_i = t_i - t_{i-1} \ \forall \ i > 0$. The filtered error trace is then given by $\{t_i \ \forall \ \tau_i > T\}$ for some threshold T. From Fig. 4, we see that the Fano factor scales with window size for large window sizes. For window sizes of less than about 50 b, we see that the Fano factor is constant and close to unity. Hence, a short section of errors may be modeled as a Bernoulli process, but a longer section requires a model that accounts for clustering. Since our interest in this section is in understanding the longer timescale clustering of errors, we proceed by filtering out the short timescale errors. The rest of the analysis in this section is presented on the filtered error traces with $T = 50$ b.

The interval serial correlation coefficient $\sigma(k)$ is a measure of dependence between intervals at lag k in a point process

$$\sigma(k) = \frac{\mathbb{E}[\tau_i \tau_{i+k}] - \mathbb{E}[\tau_i]^2}{\mathbb{E}\left[(\tau_i - \mathbb{E}[\tau_i])^2\right]} \tag{2}$$

where $\mathbb{E}[\cdot]$ is the expectation operator over i. For a renewal process, $\sigma(0) = 1$ and $\sigma(k) = 0 \ \forall \ k \neq 0$. Fig. 5 shows the measured $\sigma(k)$ as a function of k for the filtered error trace of F38S2DD. The values of $\sigma(k)$ for $k > 0$ are small. The filtered process thus shows no significant dependency between inter-error intervals as would be expected of a renewal process. Similar results are obtained for all six error traces.

The generalized Pareto (GP) distribution [12] has tail probability with fractal scaling properties. The cumulative distribut-ion function (CDF) of the GP distribution is given by

$$F(\tau) = 1 - \left(1 + \xi \frac{\tau}{\psi}\right)^{-1/\xi} \tag{3}$$

where ξ is a shape parameter and ψ is a scale parameter of the distribution. We find that the GP distribution models the probability distribution of the interval length accurately. Fig. 6 shows the estimated cumulative hazard function[1] of the interval distribution of the F38S2DD error trace along with a GP fit estimated using the `gpfit` function in MATLAB. Similar results are obtained for all six error traces.

We validate that the generalized Pareto renewal (GPR) process accurately models the long timescale errors by using the time transformation tests of Ogata [13]. The time transformation tests make use of the time-rescaling theorem [14, Th. 6]. If the model point process has an identical conditional intensity function[2] to the observed error process, then the transformed point process will be consistent with a homogeneous Poisson process with unity rate (Poisson parameter $\lambda = 1$). Ogata uses the term "residual process" to describe the transformed process. Testing on the residual process is, therefore, a test for a homogeneous Poisson process with unity rate. Berman's test [13] compares modified intervals of the residual process with a uniform distribution on $[0, 1)$. Testing requires that parameters for the GP distribution be estimated from the data. To partially alleviate the testing consequences of this estimation, we partition the data into two processes of equal size, estimate parameters from one partition, and test on the other partition. We make use of the Spike Train Analysis with R

[1]For a random variable with CDF $F(\tau)$, the cumulative hazard function can be expressed as $H(\tau) = -\log(1 - F(\tau))$.

[2]The intensity function of a point process at time t is defined as $\lim_{\Delta t \to 0} \mathbb{P}$ (one event occurs in time $[t, t + \Delta t]$)$/\Delta t$.

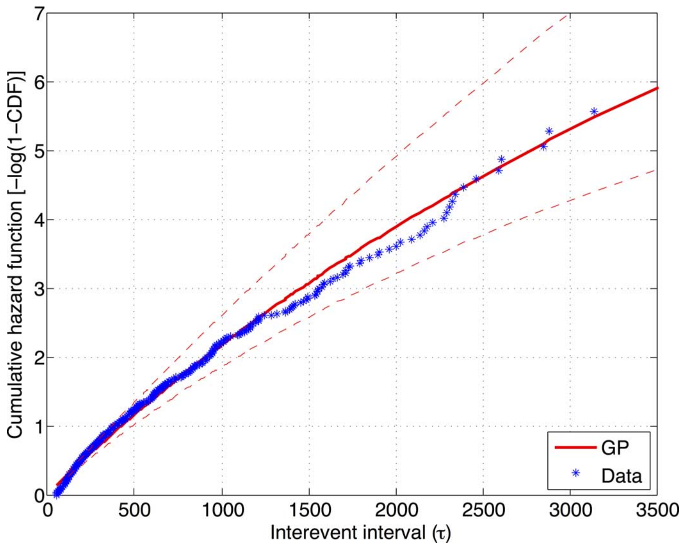

Fig. 6. Interval cumulative hazard function for a filtered F38S2DD error trace with $T = 50$ b, along with a GP fit ($\xi = 0.12, \psi = 402$) to the data. The dashed lines are the 95% confidence interval guides. The cumulative hazard plots for other filtered error traces have similar goodness of fit.

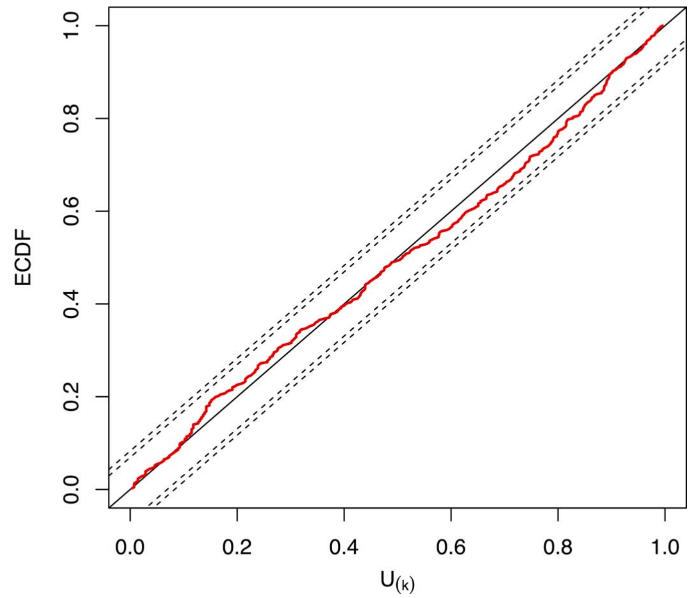

Fig. 7. Berman's test applied to the residual process after time transformation of the filtered F38S2DD error trace with $T = 50$ b. The distribution function plotted as a function of modified intervals U_k is expected to lie on a straight line. Shown here are the empirical CDF (ECDF) of the intervals from the residual process (solid red line) and the 95% and 99% confidence intervals from the Kolmogorov–Smirnov test (dashed black lines).

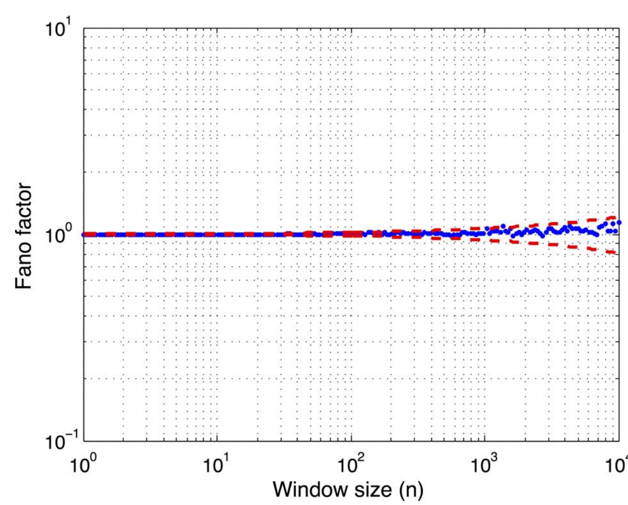

Fig. 8. Fano factor plot for the residual of the filtered F38S2DD error trace with $T = 50$ b. This plot shows that there is no significant residual clustering in the process after time transformation using a GP model; 99% confidence intervals assuming a χ^2 distribution are shown (dashed red lines).

(STAR) package to perform the tests [15]. Fig. 7 shows the result of Berman's test for the residual of the filtered F38S2DD process displayed using the style of a two-sided single sample Kolmogorov–Smirnov test. Shown with the test results are 95% and 99% confidence intervals (two sets of outer dashed lines). The test results are bounded by both of these confidence intervals. In [13], it is observed that while Berman's test is passed, it is quite possible to have clustering in the residual process. For this reason, we also show a Fano factor plot of the residual process with 99% confidence intervals in Fig. 8. The confidence intervals assume a χ^2 distribution of uncertainty in the Fano factor and are suitable for testing for a homogeneous Poisson process [16]. The Fano factor plots show that there is no significant clustering in the residual process. Ogata also suggests testing using the empirical log-survivor function and Pouzat and Chaffiol [17] suggest a Wiener process test. These additional tests were performed and the results were consistent with a GPR process.

E. Short-Term Clustering Due to Decision Feedback

Modeling of the short-term clustering due to the feedback of erroneous decisions is more difficult. We assume that the long timescale error process is a parent process that drives a short timescale daughter process. Every time the parent process generates an error, a daughter process is instantiated. This process generates a cluster of errors that lasts for a finite but random length of time. The daughter process represents the effect of the erroneous feedback in the receiver system. Although the general parent–daughter process structure is likely to be generally applicable, the exact model for the daughter process will depend strongly on the receiver structure.

It is impossible to completely separate the errors from the parent and daughter process in an error trace. However, we obtain estimates of the daughter process corresponding to each parent process event using the following technique: We mark the errors from the parent process using the filtering technique outlined in the previous section. All remaining errors in the error trace are then assigned to a daughter process corresponding to the preceding parent process error. The length of each daughter process is the number of bits between the corresponding parent process error and the last error from the daughter process.

An averaged Fano factor plot for all daughter processes derived from the F38S2DD error trace using the technique in the previous paragraph is shown in Fig. 9. At short window sizes, the Fano factor is close to unity, suggesting a Bernoulli process model at short timescales. As the window size increases beyond 20, the Fano factor systematically grows; this may at least in part

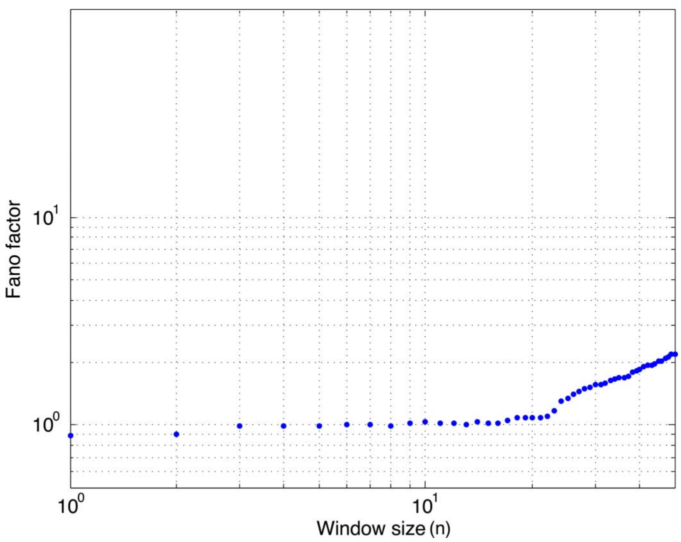

Fig. 9. An averaged Fano factor plot for all daughter processes derived from F38S2DD error trace with $T = 50$ b. The plot is consistent with a Bernoulli process at short timescales. Similar results are obtained for other error traces.

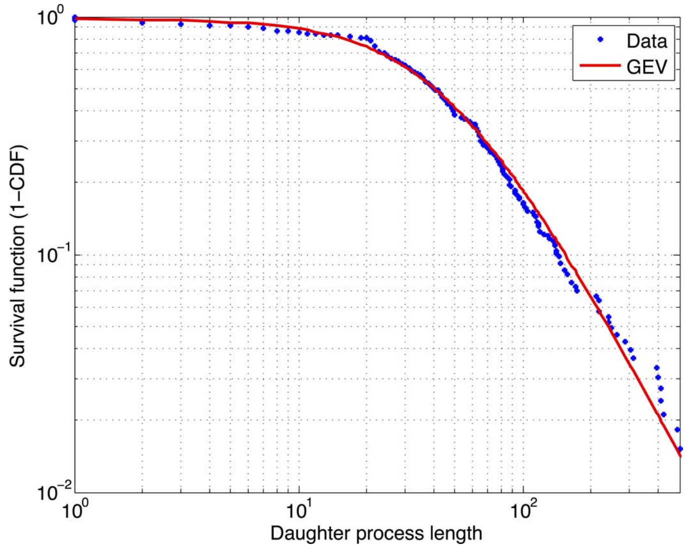

Fig. 10. Daughter length survival function (1-CDF) for a F38S2DD error trace with $T = 50$ b, along with a GEV fit ($\xi = 0.54$, $\psi = 29$, $\mu = 28$) to the data. Similar goodness of fit is obtained for other error traces.

be attributed to contamination from the parent process and from the truncation of the daughter process due to the filtering. Recall that the filtering was performed with $T = 50$ b and, therefore, one would expect significant deviation as the window size approaches 50. Similar results are obtained for all six error traces. Although it is plausible that the errors of the daughter process exhibit weak inherent clustering, we cannot test for this since our estimated parent–daughter separation of observed data is not perfect.

The probability distribution of the length of the daughter process was empirically derived from the F38S2DD error trace. By testing several common probability distributions, we found that the generalized extreme value (GEV) distribution [18] offered the best fit. The CDF of the GEV distribution is given by

$$F(z) = \exp\left[-\left(1 + \xi\frac{z-\mu}{\psi}\right)^{-1/\xi}\right] \tag{4}$$

where ξ is a shape parameter, ψ is a scale parameter, and μ is a location parameter. The survival function[3] (also known as the tail distribution or the complementary CDF) estimated from the data and the best fit GEV computed using the `gevfit` function in MATLAB are shown in Fig. 10. Similar results are obtained for other error traces.

Although one may expect that the Bernoulli error probability b in a daughter process could be estimated by counting the number of correct and erroneous bits in all daughter processes, as a result of the contamination from the parent process, this procedure overestimates b by a factor of two to three. For the SPACE'08 data sets, this procedure yielded $b = 0.06$ but the best model match is obtained for $b = 0.03$. To estimate b

[3]For a random variable with CDF $F(\tau)$, the survival function $S(\tau) = 1 - F(\tau)$.

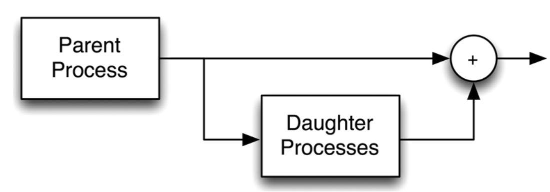

Fig. 11. Block diagram of the overall error generation process model.

from a data set, we recommend that this counting procedure be used for an initial estimate of b. The value of b should then be iteratively decreased until the modeled packet error probability versus packet length curve matches the measured curve from the data set. One may further formalize this procedure to vary b to minimize the mean square error between the modeled packet error probability curve and data.

III. Error Process Model

A. Statistical Model

Based on the findings discussed in Section II, we propose a statistical model for bit errors in an underwater communication stream. The model consists of a parent process and a number of daughter processes, as shown in Fig. 11. The parent process is a GPR process that generates errors at intervals drawn from a GP distribution. Each error due to the parent process additionally triggers a daughter process with a finite lifetime drawn from a GEV distribution. During the life of the daughter process, she generates additional errors in accordance with a Bernoulli process.

The model is characterized by six parameters: ξ_1 and ψ_1 for the GP distribution; ξ_2, ψ_2, and μ_2 for the GEV distribution; and the error probability b for the Bernoulli distribution. A simple algorithm to generate errors according to this error process model is given in Algorithm 1.

Algorithm 1: Algorithm to generate errors according to the proposed error process model.

Require: Model parameters: ξ_1, ψ_1, ξ_2, ψ_2, μ_2, b
Require: N is the number of events to simulate
Ensure: π is a set of error locations

$t \leftarrow 0$
$\pi = \emptyset$
for $i = 1 \rightarrow N$ **do**
  $\tau \leftarrow$ random number drawn from GP(ξ_1, ψ_1)
  $t \leftarrow t + \tau$
  $\pi \leftarrow \pi \cup \{\lfloor t \rceil\}$
  $\lambda \leftarrow$ random number drawn from GEV(ξ_2, ψ_2, μ_2)
  for $j = 1 \rightarrow \lfloor \lambda \rceil$ **do**
    $v \leftarrow$ uniform random number between 0 and 1
    if $v < b$ **then**
      $\pi \leftarrow \pi \cup \{t + j\}$
    end if
  end for
end for

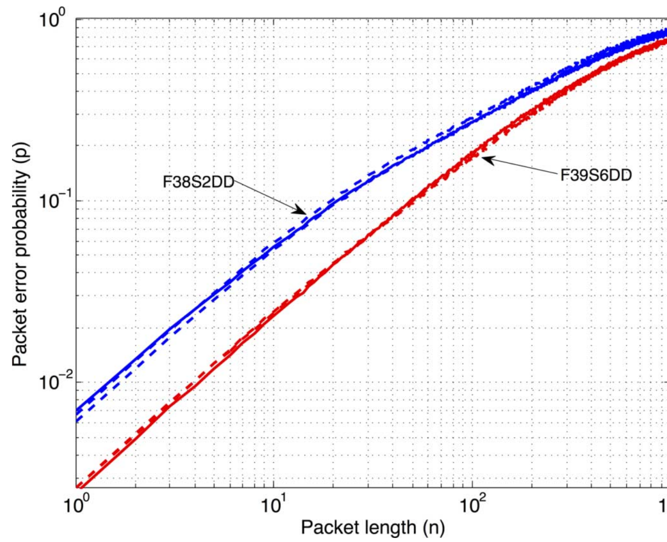

Fig. 12. Probability of packet error for two decision-directed error traces (one each from the 80-m and 1-km channels). The solid line shows the estimated packet error probability from the error trace, while the dashed lines show corresponding packet error probabilities from two simulation runs of the proposed error model.

To estimate the model parameters from an experimental data set, we first filter the error process to obtain an estimate of the parent process as described in Section II-D. We then estimate ξ_1 and ψ_1 using MATLAB's `gpfit` function on the interval distribution of the filtered process. Next, we estimate daughter lengths from the unfiltered error process, using the procedure described in Section II-E. We then estimate ξ_2, ψ_2, and μ_2 for the GEV distribution using the empirical probability distribution of the daughter length and MATLAB's `gevfit` function. Finally, we estimate b, using the procedure described at the end of Section II-E.

B. Packet Error Statistics

To validate our model, we simulate error traces in a communication stream with 10^6 b using Algorithm 1. By dividing each bit steam into nonoverlapping packets of length n, we compute the packet error probability p for the simulated error trace as a function of n. For the two data sets previously analyzed in Fig. 3, we compare the packet error probability curves from the experimental error traces and two simulation runs. The simulation for each of the data set uses model parameters estimated from the data set. As seen in Fig. 12, the simulated packet error curves closely matched the measured curves. The proposed error process model generates errors with appropriate clustering to yield the observed packet error probability for any packet length.

C. Second-Order Statistics

So far we have shown that, for a given packet length, the PER from the model matches the experimentally measured PER accurately. We next demonstrate that the model can also be used to yield a good match in second-order statistics.

Let p be the probability of packet error, i.e., $p = \Pr\{\text{packet } i \text{ is in error}\} \ \forall \ i$. Let q be the probability that two consecutive packets are in error, i.e., $q = \Pr\{\text{packet } i \text{ is in error} \wedge \text{packet } (i+1) \text{ is in error}\} = p\tilde{p}$, where $\tilde{p} = \Pr\{\text{packet } (i+1) \text{ is in error} \mid \text{packet } i \text{ is in error}\}$. We define a normalized dependency $\Omega = q/p^2 = \tilde{p}/p$. If packet errors are independent, then $\tilde{p} = p$ and $\Omega = 1$. With clustering of bit errors, one would expect that the packet errors for closely spaced packets would not be independent, with $\tilde{p} > p$. Thus, for clustered packet errors, we would expect $\Omega > 1$.

For a given packet length n, normalized dependency Ω can easily be estimated from an error trace by counting the occurrences of consecutive errors. We compare estimates of Ω from experimental and simulated error traces to check if this second-order statistic of the error process is accurately captured by our model. The result for data set F38S2DD is shown in Fig. 13. There is a good match between simulation and experiment, except in the case of extremely short packet lengths (few bits). Similar results are obtained for the other data sets.

IV. Further Experimental Validation

The proposed model is intuitively appealing and provides a good match for the data sets from the SPACE'08 experiment. Yet, additional validation based on other experimental data sets should be applied. We tested error traces from two other shallow-water experiments: RACE'08 and ROMANIS'10. We also processed the data from SPACE'08, using a different receiver structure. In this section, we present the results from these tests.

A. RACE'08 Data

The RACE'08 experiment took place in Narragansett Bay, RI, USA, in March 2008. The transmitter was mounted on a rigid tripod 4 m above the sea bottom in a 9-m water depth. The transmitted signal was a 10-kb/s, 1-min-long, BPSK-modulated pseudorandom data with a carrier frequency of 13 kHz.

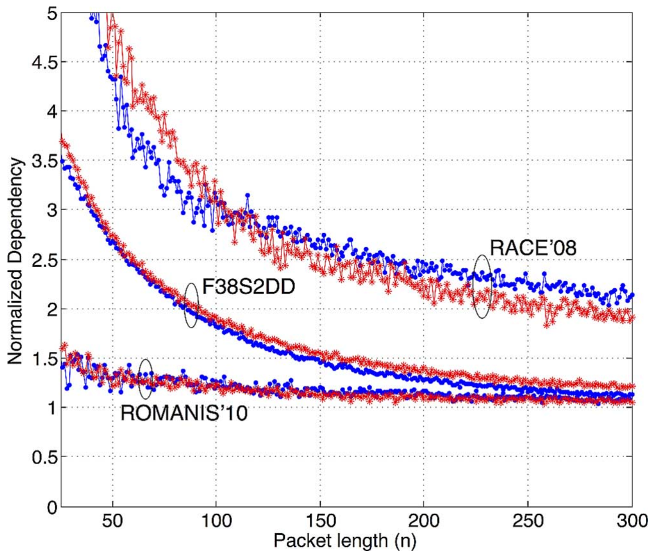

Fig. 13. Normalized dependency Ω for F38S2DD, RACE'08, and ROMANIS'10 error traces. The blue lines with round markers show the experimentally obtained values of Ω as a function of packet length n. The red lines with star markers show the simulated values of Ω using the model parameters appropriate for each data set.

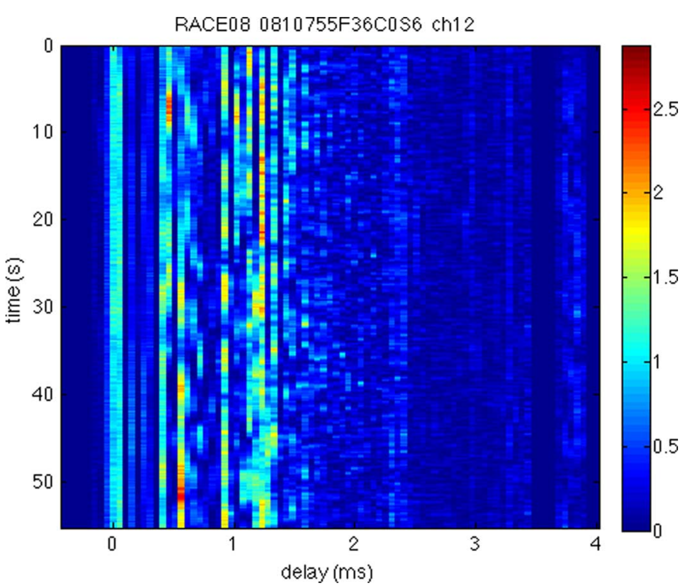

Fig. 14. Representative impulse response from the RACE'08 experiment. The horizontal axis represents multipath delay and the vertical axis represents absolute time. The colorbar is in a linear scale. The snapshots are generated at the bit rate.

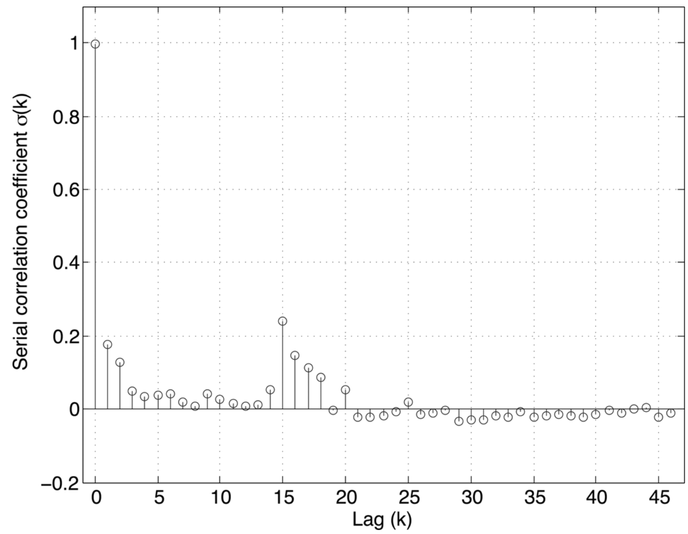

Fig. 15. Interval serial correlation coefficient $\sigma(k)$ for a filtered RACE'08 error trace with $T = 50$ b. The serial correlation coefficient shows slight residual correlation near lag 15.

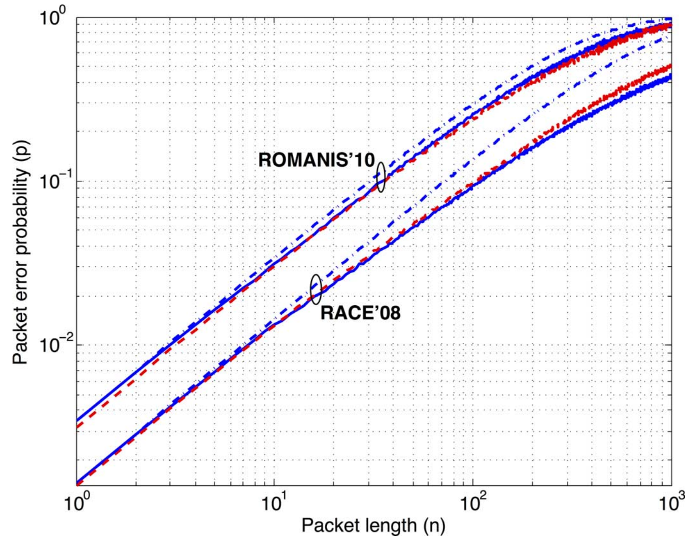

Fig. 16. Probability of packet error for RACE'08 and ROMANIS'10 error traces. The blue solid lines show the estimated packet error probabilities from the error traces, while the red dashed lines show the corresponding packet error probabilities from a simulation run of the error process model. The blue dashed–dotted lines show predicted packet error probabilities using a simple Bernoulli error model for comparison.

The receiver was a 12-sensor vertical line array with 12-cm intersensor spacing mounted on a 2-m-high rigid tripod in a water depth of 10 m. The horizontal range between the transmitter and the receiver was 1 km. Representative impulse responses for the channel are shown in Fig. 14. Received data from channel 12 was processed using the CEB–DFE with RLS algorithm used in Section II. The resulting error trace was 5.4×10^5 b in length.

We estimated the parent and daughter processes using $T = 50$ b. The interval distribution for the parent process was well modeled by a GP distribution with $\xi = 0.53$ and $\psi = 495$. The distribution, however, showed a slight interval serial correlation, as shown in Fig. 15. Whether this correlation was due to contamination from the daughter processes is unclear. The daughter process length distribution was well modeled by a GEV distribution with $\xi = 0.49$, $\psi = 13$, and $\mu = 14$. The Bernoulli probability b of the daughter processes was estimated to be 0.014. A packet error curve generated through simulation using this model follows the measured packet error curve from the data closely, as shown in Fig. 16. The match between normalized dependency curves for the measured and simulated data is shown in Fig. 13.

B. ROMANIS'10 Data

The ROMANIS'10 experiment was conducted in the area of Selat Pauh in Singapore waters on April 21, 2010. Both the

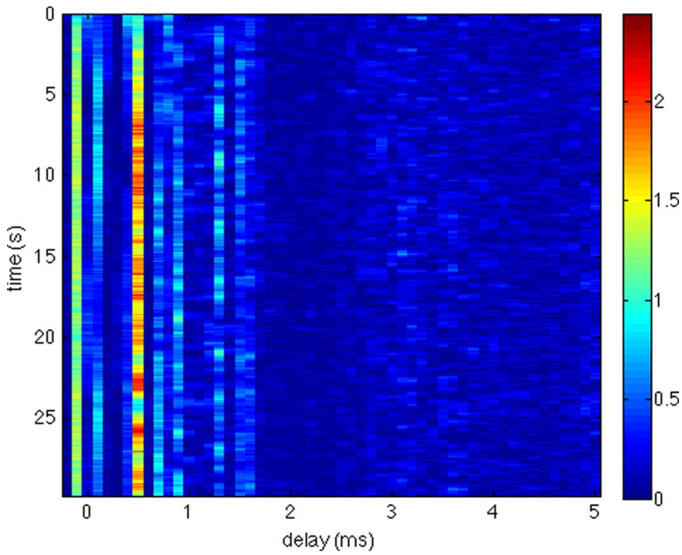

Fig. 17. Representative impulse response from the ROMANIS'10 experiment. The horizontal axis represents multipath delay and the vertical axis represents absolute time. The colorbar is in a linear scale. The snapshots are generated at the bit rate.

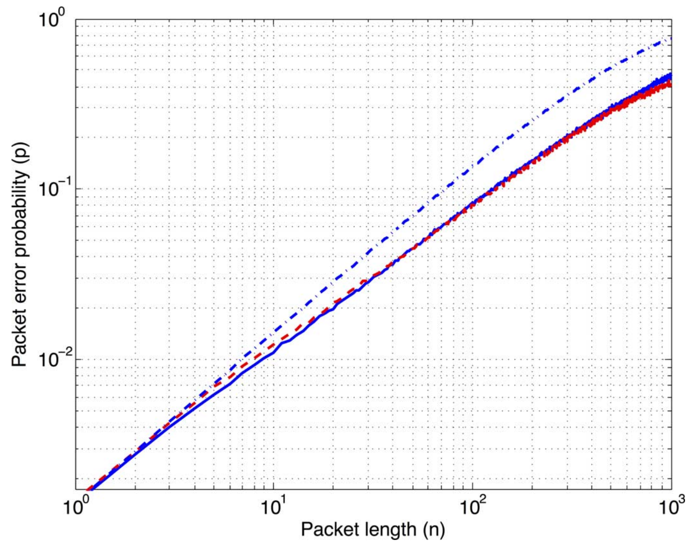

Fig. 18. Probability of packet error for SPACE'08 CEB–DFE/IPAPA error trace. The blue solid line shows the estimated packet error probability from the error trace, while the red dashed line shows the corresponding packet error probability from a simulation run of the error process model. The blue dashed–dotted line shows predicted packet error probability using a simple Bernoulli error model for comparison.

transmitter and the receiver were mounted on rigid tripods, 4 m above the seafloor. The water depth was 15 m and the horizontal range of the link was 350 m. The transmitted signal was a 5-kb/s rate, BPSK-modulated pseudorandom data with carrier frequency of 27.5 kHz. Representative impulse responses for the channel are shown in Fig. 17. A notable feature of this channel was a broadband interference from an unknown source arriving every 10 ms at the receiver. The data were processed using the CEB–DFE with the RLS algorithm.

We estimated the parent and daughter processes using $T = 50$ b. The interval distribution for the parent process was well modeled by a GP distribution with $\xi = 0.03$ and $\psi = 400$ with no significant interval serial correlation. We modeled the daughter process by a GEV distribution with $\xi = 1.05, \psi = 10$, and $\mu = 8$, and Bernoulli probability $b = 0.006$. A packet error curve generated through simulation using this model compares well with the measured packet error curve from the data, as shown in Fig. 16. The match between normalized dependency curves for the measured and simulated data is shown in Fig. 13.

C. SPACE'08 Data With IPAPA

In Section II, we presented results for the SPACE'08 experiment data processed with CEB–DFE using the RLS algorithm. It is plausible to check if the proposed model is robust to changes of the receiver structure. Next, we present results for the F38S6DD data set processed with CEB–DFE using the improved proportionate affine projection algorithm (IPAPA) [9]. Diversity combining was used to avail the spatial diversity from two receivers in this data set.

As the Fano factor for error traces in training mode in this data set showed deviation from 1 at smaller window sizes of about 20 b, we estimated the parent and daughter processes using $T = 20$ b. The interval distribution for the parent process was well modeled by a GP distribution with $\xi = 0.56$ and $\psi = 588$ with no significant interval serial correlation. The daughter process was well modeled by a GEV distribution with $\xi = 0.76, \psi = 6$, and $\mu = 6$, and Bernoulli probability $b = 0.058$. A packet error curve generated through simulation using this model compares well with the measured packet error curve from the data, as shown in Fig. 18.

V. Discussion and Conclusion

We analyzed six different error traces derived from 1-min-long recordings at ranges of 80 m and 1 km during the SPACE'08 experiment. We showed that packet error probability computations using an average bit error rate derived from the error traces and a Bernoulli error process assumption were inconsistent with experimentally measured PER. The mismatch was found to be primarily due to clustering of errors that occurs at several timescales. Based on the analysis of the clustering, we proposed a two-part statistical error model. The model consisted of a GPR parent process that drives Bernoulli daughter processes with GEV distributed lifetimes. We presented an algorithm to simulate communication errors using this error process model and showed that the simulated PER accurately matches the experimentally observed PER. We also showed that second-order statistics of the simulated error traces agree closely with experimental measurements. We conclude that the error process model we proposed captures the important aspects of the error generation process for DFE-based underwater communication systems.

The GPR process is a fairly general fractal renewal point process. Although our error traces were obtained from a coherent single-carrier communication system using CEB–DFE, we believe that this GPR process model is general enough for use with other receiver structures as well. This belief is further strengthened by noting that renewal processes with Pareto-distributed intervals have previously been used to model other channels and receivers [19], [20].

The Bernoulli daughter process with GEV distributed lifetimes seems more empirical and perhaps specific to the receiver structure or the experimental setup we used. However, since the daughter process operates over very short timescales, the errors generated by this process are often contained within a single packet for typical packet lengths of interest. Since the driving parent process already corrupts the packet that contains the daughter process errors, the exact structure of the daughter process error cluster becomes unimportant in the analysis of packet error performance. Packet loss computations can, therefore, be expected to be relatively robust to model mismatch in the daughter process.

In addition to the six error traces from the SPACE'08 experiment that we initially analyzed, we validated the proposed model using error traces from the RACE'08 and ROMANIS'10 experiments, and an error trace from the SPACE'08 experiment, using a different receiver structure. Even when the experimental data showed a small degree of statistical mismatch with the parent or daughter process models, the simulation results using the combined model closely approximated the observed packet error probability curves. We believe that the observed mismatch is caused by contamination of the filtered parent process by some residual daughter errors. Nevertheless, the good match in packet error probability suggests that the process model may be usefully applied in wide variety of conditions. We have limited our exploration to DFE-based single-carrier communication systems in shallow waters. We anticipate that the methodology used in this paper is more widely applicable, and therefore plan to test the model in other environmental conditions and receiver structures. The technique may also be applied to modeling of errors from a communication system with forward error correction (FEC) codes by letting b in (1) be measured at the output of the decoder, but we have not tested this. We plan to include receiver structures with FEC in our future studies.

In our work, we assumed a stationary error process model. This assumption is reasonable at short-to-medium timescales (in the order of minutes); at much longer timescales, the channel conditions may vary significantly. We observed hints of this effect in some of our longer error traces. The proposed process model can be easily adapted for this situation by allowing the parameters of the parent and daughter processes to vary over time. Although such error traces are easy to simulate, one needs a model for the variation in process parameters. Long-term communication measurements currently being undertaken will help explore this idea further.

Finally, we note that it would be useful for researchers to have representative parameter sets to use for simulation of various underwater channels (e.g., shallow water, deep water, etc.). Comprehensive analysis of data from a large number of experiments in various channels could be undertaken in the future to tabulate such parameter sets.

Acknowledgment

The authors would like to thank Dr. J. C. Preisig for conducting the SPACE'08 and RACE'08 experiments that provided valuable data for this work. The authors would also like to thank Dr. V. Pallayil and Unnikrishnan K. C. for their leadership and help during the ROMANIS'10 experiment.

References

[1] S. Shahabudeen, M. A. Chitre, M. Motani, and Y. S. Low, "Unified simulation and implementation software framework for underwater MAC protocol development," in *Proc. IEEE/MTS OCEANS Conf.*, Biloxi, MS, USA, Oct. 2009.

[2] C. Petrioli, R. Petroccia, J. Shusta, and L. Freitag, "From underwater simulation to at-sea testing using the ns-2 network simulator," in *Proc. IEEE OCEANS Conf.*, Santander, Spain, Jun. 6–9, 2011, DOI: 10.1109/Oceans-Spain.2011.6003638.

[3] R. Masiero, S. Azad, F. Favaro, M. Petrani, G. Toso, F. Guerra, P. Casari, and M. Zorzi, "DESERT Underwater: An NS-miracle-based framework to design, simulate, emulate and realize test-beds for underwater network protocols," in *Proc. IEEE OCEANS Conf.*, Yeosu, Korea, 2012, DOI: 10.1109/OCEANS-Yeosu.2012.6263524.

[4] M. Chitre, "The UNET-2 modem – An extensible tool for underwater networking research," in *Proc. IEEE OCEANS Conf.*, Yeosu, Korea, 2012, DOI: 10.1109/OCEANS-Yeosu.2012.6263431.

[5] F. Guerra, P. Casari, and M. Zorzi, "World ocean simulation system (WOSS): A simulation tool for underwater networks with realistic propagation modeling," in *Proc. 4th ACM Int. Workshop Underwater Netw.*, New York, NY, USA, 2009, pp. 4:1–4:8.

[6] F. Pignieri, F. De Rango, F. Veltri, and S. Marano, "Markovian approach to model underwater acoustic channel: Techniques comparison," in *Proc. IEEE Military Commun. Conf.*, Nov. 2008, DOI: 10.1109/MILCOM.2008.4753161.

[7] B. Tomasi, P. Casari, L. Finesso, G. Zappa, K. McCoy, and M. Zorzi, "On modeling JANUS packet errors over a shallow water acoustic channel using Markov and hidden Markov models," in *Proc. IEEE Military Commun. Conf.*, Nov. 2010, pp. 2406–2411.

[8] U. Fano, "Ionization yield of radiations. II. The fluctuations of the number of ions," *Phys. Rev.*, vol. 72, no. 1, pp. 26–29, 1947.

[9] K. Pelekanakis and M. Chitre, "New sparse adaptive algorithms based on the natural gradient and the L_0-norm," *IEEE J. Ocean. Eng.*, vol. 38, no. 2, pp. 323–332, Apr. 2013.

[10] S. Lowen and M. Teich, *Fractal-Based Point Processes*. New York, NY, USA: Wiley-Blackwell, 2005, ch. 7, pp. 153–169.

[11] S. Lowen and M. Teich, "Estimation and simulation of fractal stochastic point processes," *Fractals*, vol. 3, no. 1, pp. 183–210, 1995.

[12] B. Arnold, "Pareto and generalized Pareto distributions," in *Modeling Income Distributions and Lorenz Curves*, ser. Economic Studies in Equality, Social Exclusion and Well-Being. New York, NY, USA: Springer-Verlag, 2008, vol. 5, pp. 119–145.

[13] Y. Ogata, "Statistical models for earthquake occurrences and residual analysis for point processes," *J. Amer. Stat. Assoc.*, vol. 83, no. 401, pp. 9–27, Mar. 1988.

[14] F. Papangelou, "Integrability of expected increments of point processes and a related random change of scale," *Trans. Amer. Math. Soc.*, vol. 165, pp. 483–506, Mar. 1972.

[15] C. Pouzat, "STAR: Spike Train Analysis with R," R package ver. 0.3-5, 2012 [Online]. Available: http://cran.r-project.org/package=STAR

[16] U. Eden and M. Kramer, "Drawing inferences from Fano factor calculations," *J. Neurosci. Methods*, vol. 190, no. 1, pp. 149–152, 2010.

[17] C. Pouzat and A. Chaffiol, "On goodness of fit tests for models of neuronal spike trains considered as counting processes," Sep. 2009 [Online]. Available: http://arxiv.org/abs/0909.2785

[18] S. Coles, *An Introduction to Statistical Modeling of Extreme Values*. New York, NY, USA: Springer-Verlag, 2001, sec. 3.1.3, pp. 47–49.

[19] J. Berger and B. Mandelbrot, "A new model for error clustering in telephone circuits," *IBM J. Res. Develop.*, vol. 7, no. 3, pp. 224–236, 1963.

[20] B. Mandelbrot, "Self-similar error clusters in communication systems and the concept of conditional stationarity," *IEEE Trans. Commun. Technol.*, vol. 13, no. 1, pp. 71–90, Mar. 1965.

Mandar Chitre (S'04–M'04–SM'11) received the B.Eng. and M.Eng. degrees in electrical engineering from the National University of Singapore (NUS), Singapore, in 1997 and 2000, respectively, the M.Sc. degree in bioinformatics from the Nanyang Technological University (NTU), Singapore, in 2004, and the Ph.D. degree in electrical engineering from NUS in 2006.

From 1997 to 1998, he was with the Acoustic Research Laboratory (ARL), NUS. From 1998 to 2002, he headed the Technology Division of a regional telecommunications solutions company. In 2003, he rejoined ARL, initially as the Deputy Head (Research) and is now the Head of the laboratory. He also

holds a joint appointment with the Department of Electrical and Computer Engineering, NUS, as an Assistant Professor. His current research interests are underwater communication networks, underwater acoustic signal processing, and marine robotics.

Dr. Chitre has served on the technical program committees of the IEEE OCEANS Conference, the International Conference on Underwater Networks and Systems (WUWNet), and Defence Technology Asia (DTA) Conference and has served as reviewer for many international journals. He was the chairman of the student poster committee for the 2006 IEEE OCEANS Conference in Singapore, and the chairman for the Singapore Autonomous Underwater Vehicle Challenge 2013. He is currently an IEEE Technology Committee Co-Chair of Underwater Communication, Navigation & Positioning.

Konstantinos Pelekanakis (S'06–M'09) received the Diploma from the Department of Electronic and Computer Engineering, Technical University of Crete, Chania, Greece, in 2001 and the M.Sc. and Ph.D. degrees in mechanical and ocean engineering from the Massachusetts Institute of Technology (MIT), Cambridge, MA, USA, in 2004 and 2009, respectively.

Currently, he is a Research Fellow with the Acoustic Research Laboratory (ARL), National University of Singapore (NUS), Singapore. His current research lies in the areas of multiple-input–multiple-output (MIMO) underwater acoustic communications, and learning algorithms for sparse system identification.

Matthew Legg (M'06) received the B.Sc. (honors) degree in physics from Curtin University of Technology, Bentley, W.A., Australia, in 2000, the M.Sc. degree in applied physics from the University of South Australia, Adelaide, S.A., Australia, in 2005, and the Ph.D. degree from the Centre for Marine Science and Technology (CMST), Curtin University of Technology, in 2010.

He worked as a professional scientist and research scientist with the Defence Science and Technology Organisation (DSTO) in submarine sonar and signal processing from 2000 until 2012. In 2012, he joined the Acoustic Research Laboratory (ARL) at the National University of Singapore (NUS) as a Research Fellow. In 2013, he returned to Australia as an independent researcher to continue studying snapping shrimp noise in Australian waters. His research interest is to understand when and why impulsive noises occur in the ocean.